On the kinetics and equilibria of plasma-based dry reforming of methane

On the kinetics and equilibria of plasma-based dry reforming of methane.

Y. Uytdenhouwen [a,b], K. M. Bal [a], E. C. Neyts [a], V. Meynen [b], P. Cool [b], A. Bogaerts [a,*]

[a] Research Group PLASMANT, Department of Chemistry, University of Antwerp, Universiteitsplein 1, Wilrijk B-2610, Belgium

[b] Laboratory of Adsorption and Catalysis, Department of Chemistry, University of Antwerp, Universiteitsplein 1, Wilrijk B-2610, Belgium

*Corresponding author:
Annemie Bogaerts
Universiteitsplein 1, B2.09
Wilrijk B-2610, Belgium
+32 32652377
annemie.bogaerts@uantwerpen.be

Keywords:
Plasma; Dielectric barrier discharge; Dry reforming of methane; Chemical equilibrium; Chemical kinetics; Partial chemical equilibrium

Abbreviation:
A_{FID}, FID area; DBD, Dielectric barrier discharge; DRM, Dry reforming of methane; EC, Energy cost; f, Fraction of the gas mixture with the right reactivity; FID, Flame ionization detector; GC, Gas chromatograph; GC-MS, Gas chromatograph coupled to Mass spectrometer; ΔH^0_{298K}, Standard reaction enthalpy; I, Current; k, rate coefficient; n, Number of …; P, Power; PC, Personal computer; PCE, Partial chemical equilibrium; r_A, rate of formation or loss of molecule A; SEI, Specific energy input; S_n, Sample standard deviation; T, Period; t, Time; TCD, Thermal conductivity detector; $T(p,n_s)$, Student's t-distribution for sample size n_s and probability p set at 95%; U, Voltage; $\dot{V}$, Volumetric flow rate; V_m, Molare volume; x, molar fraction; x_e, Equilibrium mole fraction; X, Conversion; X_e, Equilibrium conversion; $\dot{y}$, Molar flow rate of component y;

Abstract

Plasma reactors are interesting for gas-based chemical conversion but the fundamental relation between the plasma chemistry and selected conditions remains poorly understood. Apparent kinetic parameters for the loss and formation processes of individual components of gas conversion processes, can however be extracted by performing experiments in an extended residence time range (2-75 s) and fitting the gas composition to a first-order kinetic model of the evolution towards partial chemical equilibrium (PCE). We specifically investigated the differences in kinetic characteristics and PCE state of the CO_2 dissociation and CH_4 reforming reactions in a dielectric barrier discharge reactor (DBD), how these are mutually affected when combining both gases in the dry reforming of methane (DRM) reaction, and how they change when a packing material (non-porous SiO_2) is added to the reactor. We find that CO_2 dissociation is characterized by a comparatively high reaction rate of 0.120 s^{-1} compared to CH_4 reforming at 0.041 s^{-1}; whereas CH_4 reforming reaches higher equilibrium conversions, 82% compared to 53.6% for CO_2 dissociation. Combining both feed gases makes the DRM reaction to proceed at a relatively high rate (0.088 s^{-1}), and high conversion (75.4%) compared to CO_2 dissociation, through accessing new chemical pathways between the products of CO_2 and CH_4. The addition of the packing material can also distinctly influence the conversion rate and position of the equilibrium, but its precise effect depends strongly on the gas composition. Comparing different CO_2:CH_4 ratios reveals the delicate balance of the combined chemistry. CO_2 drives the loss reactions in DRM, whereas CH_4 in the mixture suppresses back reactions. As a result, our methodology provides some of the insight necessary to systematically tune the conversion process.

1 Introduction

Plasmas offer an interesting approach to gas conversion for industrial applications [1–3]. Their highly energetic, collision-rich environment is often employed to activate highly stable compounds through (strongly endothermic) reactions, such as CO_2 splitting [4–10], dry reforming of methane (DRM) [4,11–13], and nitrogen fixation [14–16], at milder and more convenient conditions (ambient pressure and temperature) than for thermal conversion. Multiple reactor types have already been investigated, e.g. microwave discharge [17,18], dielectric barrier discharge (DBD) [5–12], and gliding arc discharge [19,20]. Altering the specific design of the DBD reactor [7,21–24], changing multiple process parameters [25], and adding (catalytic) packing materials [6,7,26–28] have all shown interesting and promising results. However, the fundamental relation between the plasma chemistry and the selected plasma conditions and reactor parameters remains poorly understood.

Many of these previous studies claimed that plasma processes may enable thermodynamically unfavourable conversions beyond the thermal limit and at higher rates than conventional thermal approaches. In spite of these promising observations, however, further optimization of plasma-based conversion processes is very difficult because their most fundamental characteristics are unknown. For thermal processes key quantities such as equilibrium constants or reaction rates of the main reaction channels are generally known and can be used to predict the yield in a given process setup. They are, however, usually not measured for plasma-based conversion processes. Most of the time, parametric studies of plasma-based gas conversions only report conversions or gas compositions at one or a limited set of residence times, which precludes elucidation of the kinetics or maximal yield, and makes it difficult to conclusively identify synergies between plasma and (catalytic) packing materials.

Despite the intrinsically nonequilibrium nature of plasmas, it is however possible to characterize a plasma-based conversion process in terms of a so-called partial chemical equilibrium (PCE) without the need to know the exact reaction schemes, as we have recently

demonstrated for CO_2 dissociation in a DBD reactor [25]. Here, we found that the concentration of CO_2, CO, and O_2 in the driven, out-of-equilibrium plasma evolves to a final composition in a similar manner as a thermal system would evolve to its equilibrium state, i.e. the same final composition is reached when starting from a pure CO_2 flow or a stoichiometric mixture of CO and O_2. The position of the PCE is specific to the discharge conditions at hand, as was also suggested by Vepřek and co-workers [29–31]. Note that in all cases the measured PCE state corresponded to a very large CO_2 conversion (up to 70% in a SiO_2-packed 455 μm reactor [25]), which would thermally only be attainable at very high temperatures (>3000 K) [4]. A simple PCE-based approach can show that the kinetics of plasma (catalysis) are different from traditional thermal kinetics, but can still be described by the same key criteria (i.e. rate coefficient and equilibrium). In contrast to thermal processes, these are however affected by more and different parameters, allowing for additional flexibility to tune the maximal conversion and rate.

The interesting observations of [25] can form the basis for more elaborate research into more complex chemistry sets, such as dry reforming of methane (DRM), where CO_2 and CH_4 are converted together into syngas and higher (oxygenated) hydrocarbons. Indeed, CH_4 reforming on its own already shows a more complex chemistry, compared to pure CO_2 conversion, since its products vary from C to H_2 to C_xH_y molecules, with thousands of reactions among them [32]. High conversions of methane up to 80% have been reported, with hydrocarbons up to C6 being detected [33–36]. Combining the chemistries of CO_2 dissociation and CH_4 reforming leads to even more possibilities towards oxygenated hydrocarbons $C_xH_yO_z$. This ability of DRM to produce economically valuable products from greenhouse gases, has made it one of the most widely investigated reactions in plasma chemistry, with varying results [12,20,23,37–40]. However, the highly complex chemistry of plasma-based DRM, combined with its technological potential, require a deeper insight into the fundamental characteristics of the process. A lot of knowledge is available from detailed reaction schemes obtained through modelling, e.g. those

in [32,41,42], but they only partially capture the complexity of experimental reactors and how set-up parameters change the overall kinetics.

In this work we will therefore investigate how the kinetics of CO_2 dissociation change upon addition of CH_4 in a DBD reactor. For this purpose, we generalise our PCE model (that was specifically developed and only applicable for CO_2 splitting) to arbitrary gas mixtures with *a priori* unknown stoichiometry. Hence, this novel method does not require knowledge on the precise process stoichiometry, and can be applied to multicomponent mixtures, also for other gas conversion applications. This approach will allow other researchers as well to compare the conversion characteristics of certain individual components across different reactors and gas mixtures.

In order to understand the occurring changes, pure CH_4 reforming will be tested and compared at the same conditions as used in our previous work on CO_2 splitting [25] being the benchmark. In this way we can elucidate how the apparent kinetics of these pure reactions are different from their combination in the DRM reaction. Also, we will evaluate the impact of a non-porous SiO_2 spheres as packing on the kinetics of CH_4 reforming and DRM, compared with CO_2 dissociation, and how the CO_2 : CH_4 ratio in DRM shifts the kinetics. Despite the simplicity of the experimental set-up, salient mechanistic insights are obtained. Eventually, information on the maximal conversion in a DBD plasma and its overall kinetics will be useful in the determination of optimal process conditions, and to compare different set-ups and packing materials on a systematic basis.

2 Methods and theory

2.1 Experimental set-up

The experiments were performed in the same set-up as in our previous work [25], as shown in Figure 1. A 455 μm gap size was used as the reference gap size, also showing the highest rate coefficients of the various gap sizes tested. We used a coaxial DBD micro gap reactor, made of an alumina dielectric tube with a precision honed inner diameter of 17.41 mm and a

wall thickness of 2.5 mm. A grounded stainless-steel rod with an outer diameter of 16.50 mm was placed in the centre of the alumina tube, to act as the inner electrode and to shape the reaction volume with a discharge gap of 455 μm. The tube was wrapped with a stainless-steel mesh over a length of 100 mm to act as the high voltage outer electrode of the DBD reactor and define the reaction zone length. The resulting reaction volume is 2.4x10^3 mm^3. Besides studying the empty reactor, the reactor was also packed with non-porous SiO_2 spheres (Sigmund Lindner) with a size range of 100-200 μm. We used a SiO_2 packing to be able to compare with our previous results for pure CO_2 splitting, and because the other packing material used in our previous work (ZrO_2) did not reach the desired 30 W (triggering the current safety switch of the power supply) in CH_4 or CO_2/CH_4 mixtures for DRM. Although many different materials have been studied in literature in packed bed DBD, we focus on SiO_2. Indeed, the inert nature of non-porous SiO_2 is beneficial to minimise any additional effects that a packing material could have on the reactor performance (e.g. catalysis), and to focus on the basic kinetics for this study. The packing was added to the reactor and vibrated for one minute via an external device to ensure the closest packing possible in a repeatable fashion. No significant material degradation was observed during the experiments.

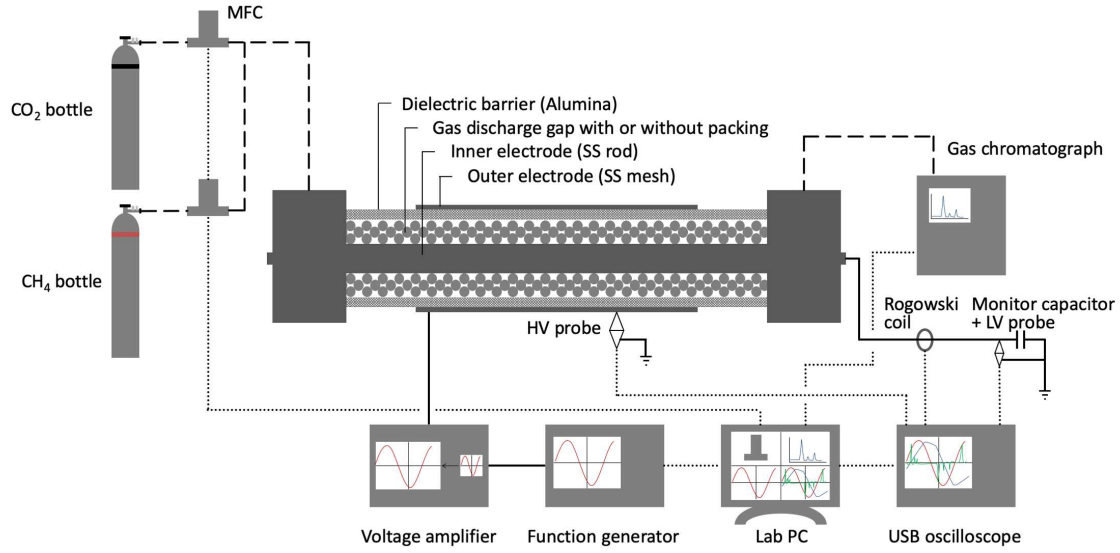

Figure 1: Micro DBD plasma reactor used in this work with analytical equipment. The reactor is not drawn to scale.

A high voltage was applied by generating a 3 kHz sine wave by a PC-controlled function generator (Tektronix, AFG 2021) and amplifying the signal with a high voltage amplifier (TREK, Model 20/20C-HS, x2000 voltage amplification). Continuous power measurements, recorded with a digital oscilloscope (Picotech, Picoscope 6402D), a high voltage probe (Tektronix, P6015A), and a current transformer (Pearson, Model 4100), were used to adjust the sine wave amplitude (between 15 and 20 kV) to obtain and maintain the desired power of 30 W. This power was measured during a number (n) of consecutive periods (T):

$$P = \frac{1}{nT}\int_0^{nT} U(t)I(t)\,dt\,. \qquad (1)$$

The reactor was fed with pure CO_2, CH_4, or a mixture of both, at different flow rates to obtain the desired residence times between 2 and 75 s in the reactor. The flow rates were set and monitored by two mass flow controllers (Bronkhorst EL-FLOW Select series). The pressure in the tubing between the reactor and the GC was kept at 1.2 bara ± 0.2 bara. In the case of the SiO_2 packed reactor, adjusted, lower flow rates were used to account for the loss in reaction volume by the packing. A packing efficiency of 49.5% was estimated, based on the computational results of our previous work for the identical case of 100-200 μm spheres in the 455 μm gap [25]. Note that we have no data point at 70 s for the SiO_2 packed DRM experiment. This point could not be measured due to the lower limit of the MFC, being 0.65 mL/min. Note that alteration of the flow rate was done to achieve different residence times, rather than changing the reactor length, in order to maintain the same power density, i.e. power-to-volume ratio, and thus constant plasma characteristics. While changing the flow rate might affect the mass and heat transfer rates, the gas temperature was estimated only slightly above room temperature (based on the measured temperature immediately after shutdown, being always below 50°C), so heat transfer should not be an issue here, like it could be in thermal reactors. The gaseous products were analysed by a gas chromatograph (Compact GC, Interscience) with pressure-less sampling. This GC has two thermal conductivity detector (TCD) channels and one flame ionization detector (FID). The first TCD channel (TCD B) contains a Rt-Q-Bond

column able to separate CO_2 and large hydrocarbons from permanent gases, the second TCD channel (TCD M) contains a Rt-Q-bond pre-column to delay CO_2 and the larger components and only inject the permanent gases on a Molsieve 5A column and separate them. The FID has a Rtx-1, 5u column to separate and detect (oxygenated) hydrocarbons. CO_2, CO, O_2, CH_4, H_2, C_2H_6, C_2H_4, C_3H_8, and C_2H_5OH were calibrated by using calibration standards (Air Liquide). More peaks could be identified but were not calibrated, since either no calibration standard was available (vapor injection identification) or they coincide with other peaks; they will not be discussed in the main text but the results are available in section 2 and 3 of the supplementary material.

The CO_2 or CH_4 conversion derived from the GC data was defined as:

$$X_y = \frac{\dot{y}_{\mathrm{in}} - \dot{y}_{out}}{\dot{y}_{in}} \qquad (2)$$

with $\dot{y}$ the molar flow rate of component y, being either CO_2 or CH_4. The total conversion was calculated according to the CO_2 : CH_4 molar ratio of the mixture, A:B, as:

$$X_{Total} = \frac{\mathrm{A}\, X_{CO_2} + B\, X_{CH_4}}{\mathrm{A+B}} \,. \qquad (3)$$

2.2 Experimental method

The standard experimental conditions in this work are set at 30 W and 3 kHz, a 455 μm discharge gap size, and 1.2 bara, at various residence times up to 75 s. The reactor was operated for at least 40 min to let it reach a thermal steady-state behaviour, i.e. a stable reactor temperature and voltage is reached due to heat losses towards the reactor and environment. Extended operating times up to 120 min were used for flow rates below 10 mL/min, to ensure steady-state behaviour in the reactor and following tubing, for consistent gas composition analysis. The applied voltage was periodically adjusted on the function generator to obtain and maintain the desired constant plasma power of 30 W. Four GC and oscilloscope measurements were recorded as soon as the steady-state behaviour from above was reached to evaluate the GC error.

Every condition was tested in three-fold for statistical review of the error, due to packing of the reactor, plasma stabilization, and random (environmental) effects. The error bars are defined as:

$$error = \pm S_n \frac{T(p,n_s)}{\sqrt{n_s}} \quad (4)$$

with S_n the sample standard deviation of the measurements, n_s the sample size, and T the two-tailed inverse of the Student's t-distribution for sample size n_s and probability p set at 95%.

2.3 Partial chemical equilibrium (PCE)

The overall reaction rate coefficient and location of the PCE are determined by applying an apparent first order reversible reaction fit to the residence time measurements. In our previous work, we explicitly derived an expression for the time evolution of molecular concentrations towards the PCE state of the CO_2/CO/O_2 system, wherein we assumed first order kinetics and stoichiometric conversion between the aforementioned molecules only [25]. Such an approach is no longer valid for more complex gas mixtures, such as those obtained for CH_4 conversion or DRM. However, a slight generalization of the equilibrium model permits its application to the conversion of any molecule in an arbitrary gas mixture, without requiring any detailed information on reaction products or mechanisms. Only first order kinetics—reaction rate proportional to the concentration of reacting molecules—is assumed. Each process could progress through many different possible individual mechanisms, between which we cannot distinguish experimentally. The measured rate coefficient is therefore a weighted average for all these individual reactions which, by construction, is assumed to be constant over time.

The loss and formation rate of a gas molecule A through unspecified pathways with rate coefficients k_{loss} and k_{form} are:

$$r_{A,\text{loss}}(x_A) = k_{\text{loss}}\, x_A \quad (5)$$

$$r_{A,\text{form}}(x_A) = k_{\text{form}}\, (1 - x_A) f. \quad (6)$$

Not all of the (non-A) molecules in the system can directly be converted into A, because only a fraction f has the "right" reactivity. We assume that f is a constant that depends on the elemental composition of the system. By construction, it is therefore a time-averaged stoichiometric parameter throughout all stages of the conversion process, just like the rate coefficient to which it is tied. Derivation of the formula, that is shown in detail in the supplementary information leads to the fit equation describing the concentration (in mole fraction) of A in time:

$$x_A(t) = x_{A,e} - \left(x_{A,e} - x_{A,i}\right) e^{-kt}, \quad (7)$$

where $x_{A,e}$ and $x_{A,i}$ are the equilibrium and initial mole fraction of A and

$$k = f k_{\text{form}} + k_{\text{loss}} \quad (8)$$

$$x_{A,e} = \frac{f k_{\text{form}}}{f k_{\text{form}} + k_{\text{loss}}}. \quad (9)$$

This equilibrium mole fraction $x_{A,e}$ can be rewritten in terms of the total equilibrium conversion $X_{Total,e}$ as:

$$X_{Total,e} = \frac{k_{loss}}{f k_{\text{form}} + k_{\text{loss}}}. \quad (10)$$

The fit was applied by importing the experimental data (consisting of up to 132 data points per parameter and reaction) into MATLAB as gas fractions, calculating a fit according to equation (7) resulting in k and x_e (converted to X_e), and finally converted back into conversions for plotting on the graphs. $x_{A,i}$ is equal to 1 for pure CO_2 and CH_4, as well as for fitting the overall DRM trend (where $x_A = x_{CO2} + x_{CH4}$), while the respective CO_2 and CH_4 fractions were taken for their individual fits in mixed DRM cases. k_{loss} and $f\,k_{form}$ are calculated from equations (8) and (9).

3 Results and discussion

3.1 The benchmark: Separate CO_2 and CH_4 conversion

CO_2 dissociation was performed in our previous work [25] at the standard conditions mentioned in the experimental method. Note that the thermodynamic equilibrium at the considered

(ambient) temperature and pressure is virtually 0% for all gas compositions (pure CO_2 and CH_4, as well as all DRM mixtures) [4]. The results, plotted as the black curve in Figure 2(a), however show that the CO_2 splitting reaction under the considered plasma conditions was characterized by an equilibrium conversion of 53.6% with an apparent overall reaction rate coefficient of 0.120 s^{-1} (Table 1), found by the apparent first order reversible reaction fit. Viewing these results through the lens of our simplified equilibrium model, and more specifically the expressions for the apparent reaction rate coefficient and equilibrium conversion in equations (8) and (9), we get a k_{loss} term of 0.066 s^{-1} and a fk_{form} term of 0.056 s^{-1}. The dominant reactions in the DBD reactor are electron-impact dissociation of CO_2 as main CO_2 loss process, while three-body recombination of CO and O is the most important formation reaction, as reported by Aerts et al. [8].

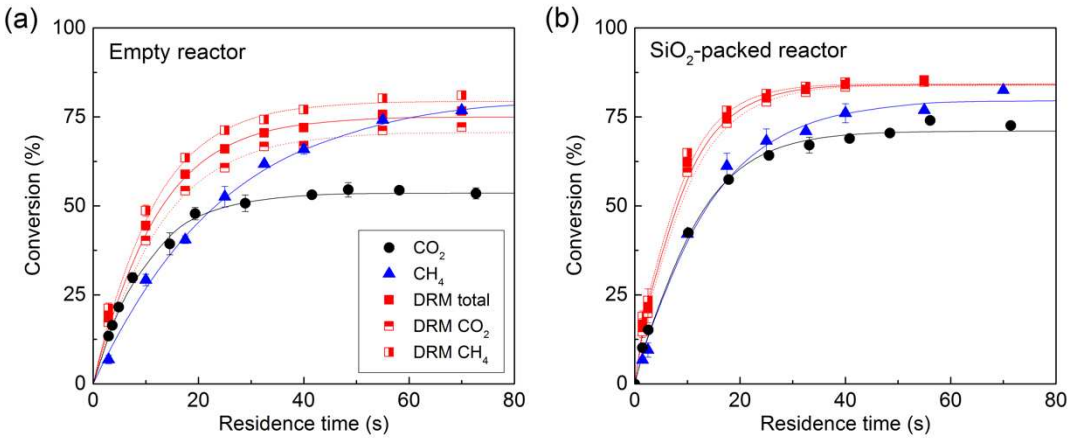

Figure 2: Conversion of CO_2 (black circles), CH_4 (blue triangles), and DRM (red squares), plotted as a function of residence time for both the empty and SiO_2-packed reactor. The individual conversion of CO_2 (horizontal half red squares) and CH_4 (vertical half red squares) during DRM are plotted as well. An apparent first-order reversible reaction fit for all reactions is applied (solid/dotted lines). The exact values can be found in Table S 1 in the supplementary material.

Table 1: Fitted kinetic and partial chemical equilibrium data for CO_2 dissocitation, CH_4 reforming, and DRM, as well as its sub-reactions, for both the empty and SiO_2-packed reactor at the standard conditions.

Reaction		CO_2 splitting [25]	CH_4 reforming	DRM total	DRM CO_2	DRM CH_4
Empty	k (s^{-1})	0.120 ± 0.005	0.041 ± 0.002	0.088 ± 0.003	0.083 ± 0.002	0.093 ± 0.003
	k_{loss} (s^{-1})	0.066 ± 0.003	0.034 ± 0.003	0.066 ± 0.003	0.059 ± 0.003	0.074 ± 0.003
	f k_{form} (s^{-1})	0.056 ± 0.003	0.0073 ± 0.0006	0.0217 ± 0.0009	0.024 ± 0.001	0.0190 ± 0.0008
	X_e (%)	53.6 ± 0.8	82 ± 2	75.4 ± 0.6	71.2 ± 0.7	79.7 ± 0.7
Si	k (s^{-1})	0.111 ± 0.004	0.074 ± 0.005	0.130 ± 0.005	0.118 ± 0.004	0.143 ± 0.006

	k_{loss} (s^{-1})	0.079 ± 0.004	0.059 ± 0.005	0.109 ± 0.005	0.099 ± 0.004	0.121 ± 0.006
	f k_{form} (s^{-1})	0.032 ± 0.002	0.014 ± 0.001	0.020 ± 0.001	0.018 ± 0.001	0.022 ± 0.001
	X_e (%)	71.1 ± 0.8	81 ± 2	84.3 ± 0.8	84.3 ± 0.8	84.4 ± 0.8

CH_4 reforming was carried out at the same conditions, and the results are shown in Figure 2(a) and Table 1 as well. They exhibit completely different behaviour from CO_2 dissociation with a higher equilibrium conversion of 82%. However, the overall apparent reaction rate coefficient of CH_4 reforming is only a third of the value for CO_2 dissociation, i.e. 0.041 s^{-1}. Our equilibrium model shows that k_{loss} and fk_{form} both have much lower values than those seen with CO_2 dissociation, being 0.034 s^{-1} and 0.0073 s^{-1} respectively (cfr. equations (8) and (9)). From our modelling work it was established that the CH_4 loss reactions in a DBD reactor are dominated by electron impact ionization and dissociation of CH_4, yielding CH_4^+ and CH_3^+ ions, as well as CH_3, CH_2, and CH radicals, cfr. equations R1-5 in [32] and Table 2 in [42]. In view of the small value of k_{loss}, these processes are therefore not as efficient as in the pure CO_2 plasma, which seems counterintuitive based on the reaction enthalpies. However, as shown by Snoeckx et al. [42], electron impact dissociation of CH_4 is very fast, but the recombination of the produced CH_x radicals back towards CH_4, is also very quick, resulting in a net low conversion and thus low effective rate coefficient. On the other hand, the products of CO_2 electron impact dissociation are more stable: CO is a saturated molecule, and the O atoms can recombine into O_2, ultimately leading to the higher effective loss rate from electron impact-driven processes.

The net CH_4 formation is mainly due to electron impact dissociation of C_3H_6 and C_3H_8 (cfr. equations R12 and R14 in [32]). These C3 hydrocarbons are however not very abundant in our CH_4 plasma, with a maximum product fraction of 2.54% measured in all our CH_4 experiments at steady state (see Table S 3 in the supplementary material). In addition, experiments in the packed reactor (section 3.3) indeed confirm that both loss and formation processes are primarily electron impact-driven. Essentially, this means that CH_4 formation is hampered by a small f factor, which leads to a smaller effective formation rate coefficient

fk_{form}, thus shifting the conversion equilibrium away from CH_4. Because the electron impact-driven processes in this system are not as efficient as in the CO_2 system, the overall evolution rate towards this high equilibrium conversion is however lower.

Note that, although the plasma chemistry processes on the microscale are inherently fast in nature (milliseconds), the conversion on the macroscale is still a rather slow process in this DBD reactor. This is due to the balance act of short and select random micro-discharges per second (with a diameter of typically 100 μm and duration of about 200 ns), in combination with reactions in the afterglow, diffusion, convection, and back reactions, resulting an overall slower conversion process, requiring about 40 s to 80 s to reach PCE, depending on the composition.

3.2 DRM: The best of both worlds

Subsequently, both gases were combined in an equimolar ratio to perform the DRM reaction at the same standard conditions (Figure 2(a) and Table 1). The combination of CO_2 and CH_4 leads to a high overall equilibrium conversion of 75.4%, associated with a high rate coefficient of 0.088 s^{-1}, which is higher than the numerical average of the individual reactions would have been. This is a manifestation of k_{loss} being high at 0.066 s^{-1}, which is the same as for CO_2 dissociation, and fk_{form} staying fairly low at 0.0217 s^{-1}. When performing a similar analysis purely on the respective concentrations of CO_2 and CH_4 in DRM, we can see that, compared to the pure gases, k_{loss,CH_4} and $f_{CH_4}k_{form,CH_4}$ are more than two times larger, whereas $f_{CO_2}k_{form,CO_2}$ is more than halved. This means that additional reaction pathways have become available for the processes producing and consuming CH_4, while CO_2 formation pathways are suppressed due to the mixing of the two gases. These observations were also predicted by kinetic modelling [42,43]. The density of O atoms is very low in the CO_2:CH_4 mixture (there is also less than 0.023% O_2, see section 3.5.3) and this limits CO_2 formation by lowering its f factor, an effect that cannot be fully compensated by new “combustion-type” reactions of CH_4. These latter reactions, however, do affect the consumption of CH_4, because it can react with species such as O^-, OH and CO_2^+. CH_4 formation benefits from the availability of more radicals

for three-body recombinations in DRM [42], hence explaining the increase of $f_{CH_4} k_{form,CH_4}$ when CO_2 is present.

These changes result in mixing of the characteristics of the individual reactions, towards the overall DRM kinetics trend seen above. In total, we effectively see CO_2 boosting the conversion rate coefficient of CH_4 while it reduces its own rate coefficient although to a smaller extent. Moreover, CH_4 addition increases the (equilibrium) conversion of CO_2 while slightly reducing its own equilibrium conversion. The overall result is that we obtain the best of both worlds in DRM, i.e. high apparent rate coefficients, like in CO_2 dissociation, and high equilibrium conversions, like in CH_4 reforming. In the most practical sense, the changes in kinetics and PCE state, resulting from mixing CO_2 and CH_4, ensure that for any "practical" (short) residence time, the DRM process significantly outperforms its pure gas counterparts in terms of obtained conversion for both compounds, as can be seen in Figure 2 (a).

It should also be noted that the individual CO_2 and CH_4 conversion in our DRM reaction, under the applied conditions here, are very close to each other, in comparison to other studies [11,12,44,45]. These papers report typical $X_{CH_4} : X_{CO_2}$ ratios between 1.5 and 2, while ours are between 1.22 and 1.12 at the shortest and longest residence time, respectively.

3.3 Tuning the kinetics by packing material

Our previous work showed that adding a packing material to the reactor can tune both the rate coefficient and equilibrium conversion of plasma-induced CO_2 dissociation individually, while at most enhancing only the rate in traditional thermal reactors (in case of a catalytic packing) [25]. These changes are usually attributed to alteration of the plasma properties by physical effects of the packing materials on the discharge [46]: When a plasma changes, also the associated PCE can change. Generally speaking, adding a packing material will increase the local electric field near the contact points, and thus increase the electron temperature, while slightly lowering densities of some species due to more surface losses, depending on the material-gap combination [47]. Indeed, the applied peak-to-peak voltage (a measure for the

reduced electric field E/N as the discharge gap remains constant and thus also for the electron temperature) increases significantly for all compositions upon adding the SiO_2 packing, see Table S 10 in the supplementary information. This should result in a boost of the electron impact reactions, i.e. the major loss reactions for CO_2 and CH_4, therefore increasing k_{loss}, k, and X_e.

A SiO_2 packing was previously found to significantly increase the CO_2 equilibrium conversion from 53.6% to 71.1%, while only slightly decreasing the rate coefficient from 0.120 s^{-1} to 0.111 s^{-1} [25], as shown when comparing Figure 2 (a) and (b) and Table 1. Indeed, k_{loss} increases because electron impact-based loss reactions are stimulated by the increased electron temperature, whereas fk_{form} does not, because three-body neutral recombinations are unaffected by the electron temperature [8]. In fact, fk_{form} even decreases, which may be explained by the larger surface/volume ratio in the packed reactor: the presence of a large surface area will facilitate surface-mediated O atom recombination, thus reducing the density of O atoms in the gas phase, and hence suppressing the formation of CO_2 along the three-body recombination pathway by lowering the f factor [48]. The opposite effect of the packing on the respective CO_2 dissociation and formation rates therefore explains how the CO_2 equilibrium conversion can increase, while its overall conversion rate coefficient slightly decreases.

The same experiments for CH_4 reforming show a (almost) doubling of both k_{loss} and fk_{form} upon packing the reactor. While the SiO_2 packing does not enhance the equilibrium conversion, the apparent rate coefficient almost doubles from 0.041 s^{-1} to 0.074 s^{-1} (see Table 1). As discussed in section 3.1, the most prominent reactions for both loss and formation of CH_4 in a DBD are again electron impact reactions–i.e. dissociation and ionization for CH_4 loss and dissociation of C_3H_6 and C_3H_8 for CH_4 formation, respectively. This means that both loss and formation are equally affected by a change in electron temperature, so that the ratio of

k_{loss} and k_{form} is constant (as well as the equilibrium conversion), but their sum (and the overall reaction rate) increases.

Finally, the addition of a SiO_2 packing in DRM increases both the total equilibrium conversion, from 75.4% to 84.3%, and the apparent total rate coefficient, from 0.088 s^{-1} to 0.130 s^{-1} (cf. Table 1). Although the individual CO_2 and CH_4 rate coefficients (0.118 s^{-1} and 0.143 s^{-1} respectively) differ more compared to the empty reactor (section 3.2), the individual equilibrium conversions become roughly equal (84.3%), which is different from the empty reactor where the CH_4 conversion remained higher that the CO_2 conversion. This results in X_{CH_4} : X_{CO_2} ratios being even closer to 1, i.e. 1.29 to 0.99 at the shortest and longest residence times, respectively. The data shows that for both CO_2 and CH_4, and thus in total for DRM as well, k_{loss} strongly increases while fk_{form} stays about the same when the packing material is added. The changes in kinetics are again expected since both CO_2 and CH_4 losses are based on electron impact reactions, resulting in a rise of k_{loss} due to the higher electron temperature in case of the SiO_2 packing. The formation reactions have been predicted to be mostly based on ion and neutral chemistry for CO_2, and three-body recombination, electron impact on C3 (which are barely present), and C2 three-body reactions for CH_4, meaning that k_{form} is almost unaffected [42,43].

3.4 Tuning the kinetics by mixing ratio

In section 3.1 we discussed how CO_2 dissociation is characterized by a high apparent rate coefficient but low equilibrium conversion, while CH_4 reforming displays a low apparent rate coefficient but high equilibrium conversion. Combining both in DRM results in total rates and conversions in between these values. In this section we look further into the mechanistic aspects of this mixing, by also testing 3:1 and 1:3 CO_2 : CH_4 ratios.

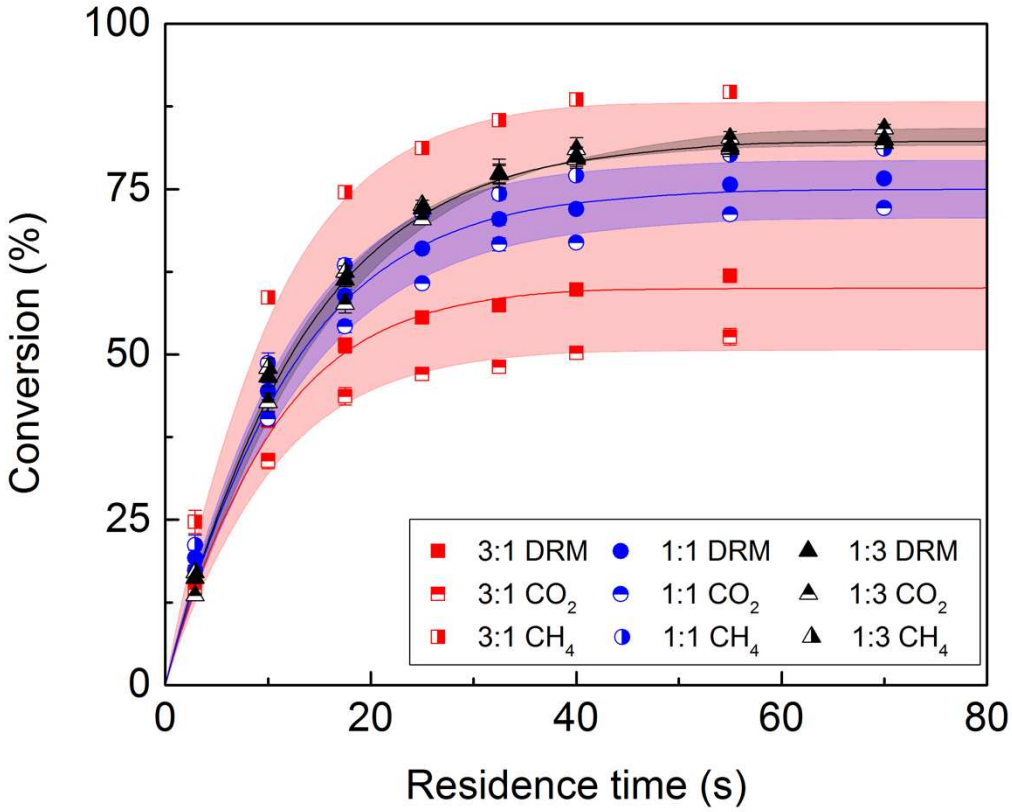

Figure 3: Total conversion of DRM with a CO_2 : CH_4 ratio of 3:1 (red squares), 1:1 (blue circles), and 1:3 (black triangles); plotted as a function of residence time in an empty reactor. The individual conversions of CO_2 (horizontal half shapes) and CH_4 (vertical half shapes) are plotted as well. Apparent first-order reversible reaction fits for all conversions are shown for the total conversion (solid lines) and the individual conversions (by the edges of the corresponding coloured regions). The exact values can be found in Table S 1 in the supplementary material.

Table 2: Fitted kinetic and equilibrium data for DRM at different CO_2 : CH_4 ratios, and for the pure CO_2 and CH_4 reactions, in an empty reactor. The fit was applied for the total conversion as well as the sub-reactions.

CO_2 : CH_4 ratio		1:0 [25]	3:1	1:1	1:3	0:1
Total	k (s^{-1})	0.120 ± 0.005	0.108 ± 0.004	0.088 ± 0.003	0.080 ± 0.002	0.041 ± 0.002
	k_{loss}	0.066 ± 0.003	0.065 ± 0.003	0.066 ± 0.003	0.066 ± 0.002	0.034 ± 0.003
	f k_{form}	0.056 ± 0.003	0.042 ± 0.002	0.0217 ± 0.0009	0.0136 ± 0.0005	0.0073 ± 0.0006
	X_e (%)	53.6 ± 0.8	60.5 ± 0.6	75.4 ± 0.6	83.0 ± 0.7	82 ± 2
CO_2	k (s^{-1})	0.120 ± 0.005	0.109 ± 0.006	0.083 ± 0.002	0.067 ± 0.003	-
	k_{loss}	0.066 ± 0.003	0.055 ± 0.004	0.059 ± 0.003	0.058 ± 0.003	-
	f k_{form}	0.056 ± 0.003	0.053 ± 0.004	0.024 ± 0.001	0.0096 ± 0.0005	-
	X_e (%)	53.6 ± 0.8	51.1 ± 0.7	71.2 ± 0.7	86 ± 1	-
CH_4	k (s^{-1})	-	0.106 ± 0.003	0.093 ± 0.003	0.085 ± 0.002	0.041 ± 0.002
	k_{loss}	-	0.094 ± 0.003	0.074 ± 0.003	0.070 ± 0.002	0.034 ± 0.003
	f k_{form}	-	0.0117 ± 0.0004	0.0190 ± 0.0008	0.0151 ± 0.0005	0.0073 ± 0.0006
	X_e (%)	-	89.0 ± 0.6	79.7 ± 0.7	82.2 ± 0.6	82 ± 2

The time evolution of the conversions shown in Figure 3–with their associated kinetic and equilibrium parameters compared to the pure gases in Table 2–further clarifies the extent of the mixing effect seen in section 3.2. The rate constants and equilibrium conversion for the different gas mixing ratios interpolates continuously, but not linearly, between those for pure CO_2 and pure CH_4. The more CO_2 is added to the mixture, the higher the overall rate coefficient is, skewed towards that of the pure CO_2 system. The equilibrium conversion, however, is mainly affected by the CH_4 concentration (i.e. skewed towards the pure CH_4 case), with higher equilibrium conversions obtained with more CH_4 in the mixture. The changes in k_{loss} and fk_{form} curiously show that as long as there is CO_2 in the mixture, the loss rate coefficient k_{loss} of DRM is constant and equal to k_{loss} of pure CO_2. At first sight, the shifts in k and X_e as a function of the $CO_2 - CH_4$ ratio may therefore seem to be fully attributable to a change of fk_{form}, which decreases with increasing CH_4 concentration. Analysis of the effective kinetics of CO_2 and CH_4 shown in Table 2 (based on their individual conversion within DRM), however, shows how these shifts of k and X_e arise. k_{loss,CO_2} is independent of the mixing ratio although slightly lower than in a pure CO_2 plasma (i.e. around 0.057 s^{-1} within error bars), while a slightly higher k_{loss,CH_4} does shift with the mixing ratio but only to some extent so that the overall k_{loss} of DRM stays constant at 0.066 s^{-1}. The formation rate coefficients for both gases generally decrease with increasing CH_4 concentration, although at the 3:1 ratio, $f_{CH_4}k_{form,CH_4}$ is lower than at the 1:1 ratio, whereas $f_{CO_2}k_{form,CO_2}$ at the 3:1 ratio is close to the value for pure CO_2. As a result, the 3:1 mixture exhibits a much higher conversion of CH_4 than of CO_2 (89.0% and 51.1%, respectively).

In the most general sense, changing the $CO_2 : CH_4$ ratio therefore mainly changes the formation aspect of the overall reaction, allowing us to tune both the kinetics as well as the PCE of DRM. From the trends in the loss and formation rates, we conclude that CO_2 drives the loss reactions in DRM, whereas the presence of CH_4 in the mixture suppresses formation

reactions. The combination of these effects results in both high equilibrium conversions and high conversion rates in DRM. Combining this knowledge with insight gleaned from the experiments with the SiO_2-packed reactor, it can be inferred that electron impact-driven processes are very efficient with CO_2, and they dominate the non-equilibrium loss processes even at fairly low CO_2 fractions (25% in our experiments). CH_4 loss is enhanced by species produced in CO_2 loss reactions which, in turn, chemically suppress CO_2 formation. To have an appreciable effect on the CO_2 conversion, the CH_4 fraction must however be sufficiently high (50% in our experiments).

Table S 10 in the supplementary material shows the applied peak-to-peak voltage for the different gas mixing ratios investigated. Because we keep the discharge gap constant, the peak-to-peak voltage can be considered as a measure for the reduced electric field, and thus for the electron temperature. In contrast to the addition of the SiO_2 packing, we see no clear correlation between this peak-to-peak voltage and the kinetic data derived in our study, for the different gas mixtures. This indicates that besides the electron temperature, additional unknown factors will have an impact as well.

3.5 How residence time and gas mixture tune product composition

Besides the CO_2, CH_4, and total conversions reported above, it is interesting to understand how these differences influence the formed products. As mentioned in section 2.1, only a number of components could be quantified, and those will be discussed here. The results of the remaining components can be found with their peak areas in the supplementary material. During the experiments with CH_4, mostly at longer residence times, we could collect small amounts of carbon deposition and highly viscous fluids. GC-MS analysis showed ppm levels of C1 to C4 acids and unidentified carbon polymers. This and the uncalibrated components will of course result in an incomplete atom balance after the reactor, which is further discussed in section 3.6.1.

3.5.1 CO_2 dissociation

The products formed in CO_2 dissociation are limited to CO, O_2, O_3, and C deposits. Only trace amounts of O_3 were detected and no C deposition was observed in or after the reactor, so these will be neglected further on. The production of CO and O_2 in the empty reactor is shown in Figure 4(a). We can see that the production of CO and O_2 respects the stoichiometric 2:1 ratio of the CO_2 splitting reaction, with CO reaching a maximum concentration of around 36% and O_2 reaching around 18%.

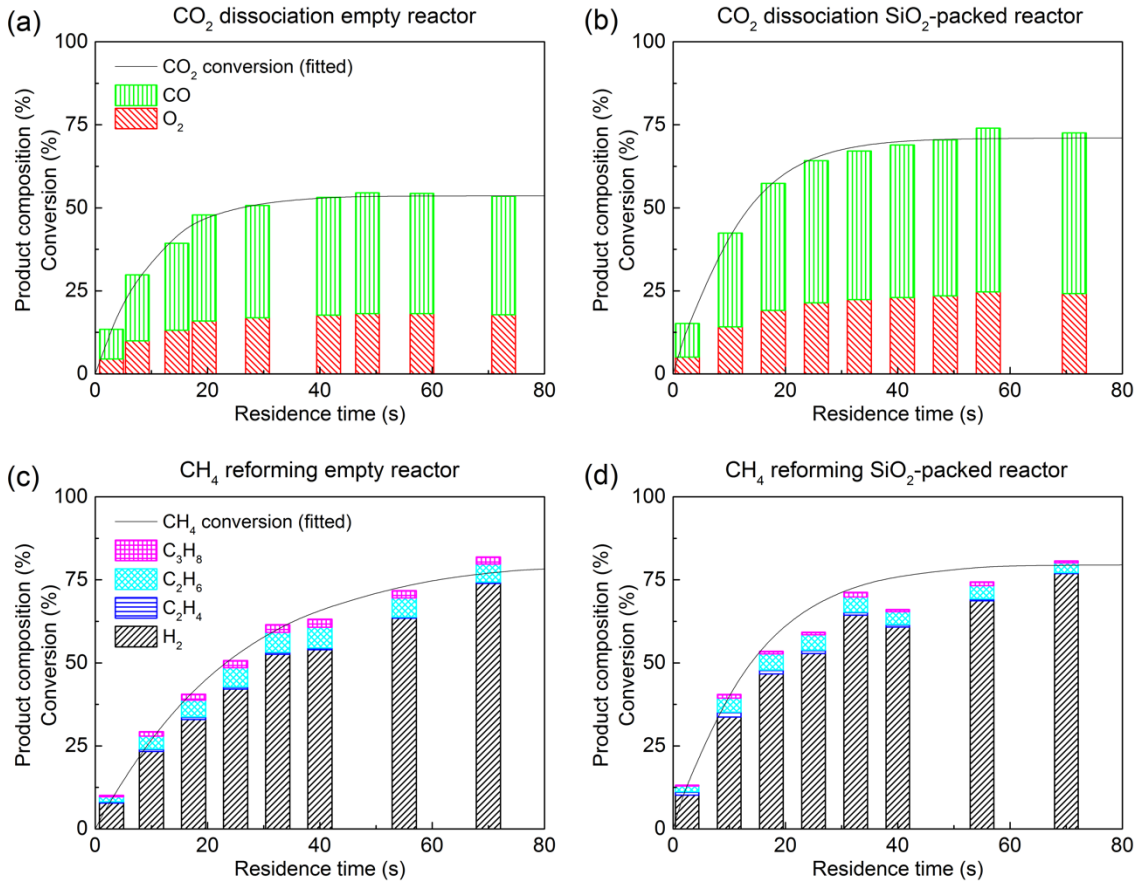

Figure 4: Measured concentration of different calibrated components after CO_2 dissociation for (a) the empty reactor and (b) the SiO_2-packed reactor, as well as after CH_4 reforming for (c) the empty reactor and (d) the SiO_2-packed reactor, plotted as stacked bars as a function of residence time. The fitted CO_2 and CH_4 conversions are displayed as well, as a reference for all cases. All components are measured on the TCD. The exact values of the concentrations can be found in Table S 3 in the supplementary material.

Adding a SiO_2 packing to the reactor enhances the conversion, as discussed in section 3.3, which also results in higher CO and O_2 concentrations, as shown in Figure 4(b). The maximum

CO concentration obtained, increases to about 49% while the O_2 concentration increases to 24%, again respecting the stoichiometric 2:1 ratio of the CO_2 splitting reaction.

3.5.2 CH_4 reforming

Figure 4(c) shows the calibrated product composition after CH_4 reforming for the empty reactor (the exact concentration of every component can again be found in Table S 3 in the supplementary material). The main component formed during CH_4 reforming is H_2, followed by ethane, propane, and ethene. A steady increase in H_2 concentration is seen from 8% to 74% upon increasing the residence time, following the increasing conversion. This trend is, however, not followed by the other components, of which the concentration first increases to a maximum value, and then decreases again. Ethane reaches a maximum concentration of 6.21% at 40 s, and slightly decreases to 5.5% at 70 s. Propane shows the same behaviour with a maximum concentration of 2.46% at 40 s, dropping to 2.1% at 70 s. Ethene reaches its maximum concentration of 0.79% already at 17.5 s, and decreases significantly to only 0.35% at 70 s. This means that these small hydrocarbons are actually intermediates that are consumed, either in the production of higher hydrocarbons or back into formation of CH_4, as well as H_2 and C, at longer residence times. Also, it can be inferred that alkenes are more prone to react further or be decomposed again, since they are more reactive.

Adding the SiO_2 packing to the reaction zone has two major effects on the product composition after CH_4 reforming. A higher share of H_2 is observed over the entire residence time range, but the changes in C2 and C3 concentration depend on the exact residence time and there are also lower amounts of all higher hydrocarbons.

3.5.3 Dry reforming of methane

Figure 5 shows the calibrated product composition for DRM. All concentrations can again be found in the supplementary material (Table S 6). The addition of CO_2 to the mixture results in high fractions of CO in the reactor effluent, as it is the main product from electron impact dissociation of CO_2. The concentration starts at 10.2% at the shortest residence time and rises

to 37.4% at the longest residence time. The other main product from CO_2 dissociation, O_2, is however barely detected; its concentration only reaches up to 0.023%. Indeed, the O atoms formed by CO_2 splitting will react further into oxygenated hydrocarbons and water, or back into CO_x, and only a small fraction recombines into O_2, whereas CO appears as one of the more stable end products of DRM. Again, we observe high concentrations of H_2, up to 39%, and producing H_2 : CO ratios close to 1 (0.91 – 1.04), see Table S 6. This syngas ratio is too low for optimal Fischer-Tropsch synthesis, where a ratio of 2 is desired [49]. Ethane, ethene, and propane show similar behaviour as seen with CH_4 reforming, i.e. a low-high-low concentration profile, but at lower values; only the ethane concentration surpasses the 1% mark, reaching 1.96% at 10 s and decreasing to 1.04%. Ethanol, the sole oxygenated hydrocarbon that could be quantified, is only formed in small amounts from 300 to 90 ppm.

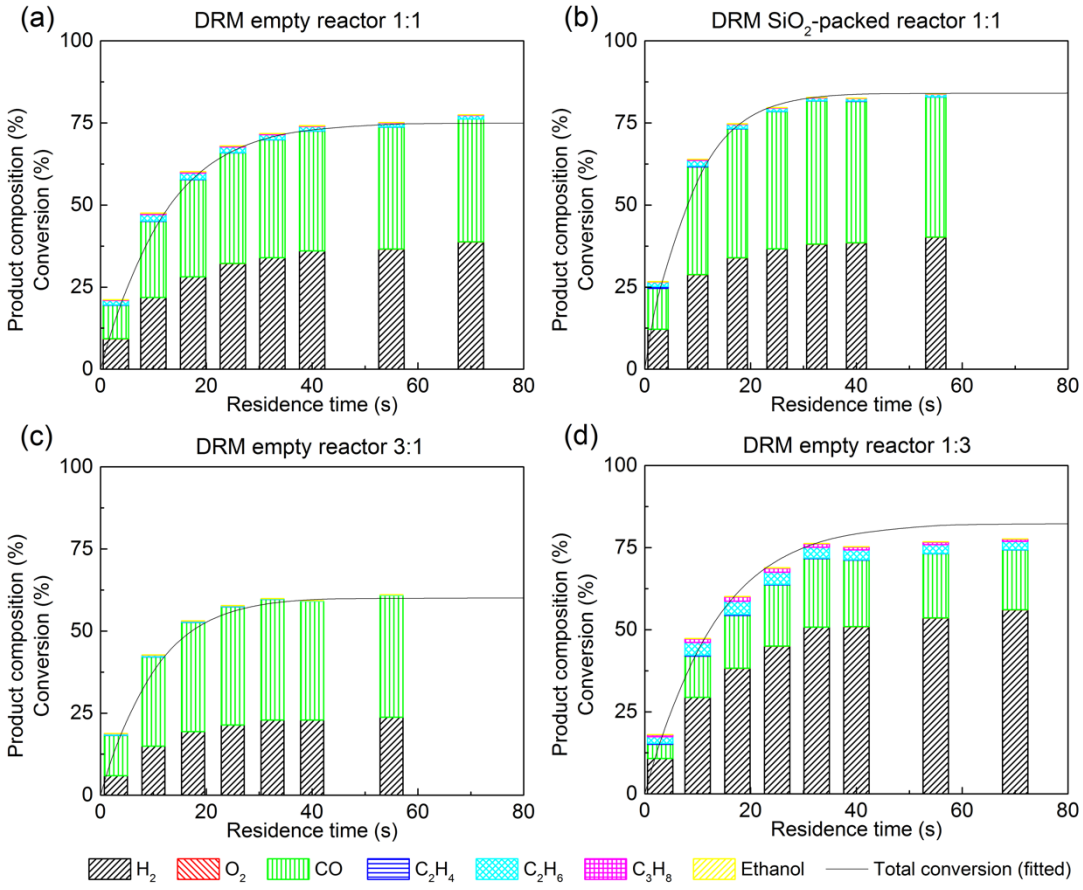

Figure 5: Measured concentration of different calibrated components for DRM, plotted as stacked bars as a function of residence time, for (a) the empty reactor with a CO_2 : CH_4 ratio of 1:1, (b) the SiO_2-packed reactor at 1:1 ratio, (c) the empty reactor at 3:1 ratio, and (d) the empty reactor at 1:3 ratio. The fitted DRM conversion is displayed as well, as a reference for each case. All components are measured on the TCD. The exact values of the concentrations can be found in Table S 6 in the supplementary material.

Although some changes can be observed in ratios of different products, adding a SiO_2 packing to the reactor does not have a large impact on the product formation. In Figure 5(b) we see that the H_2 concentration reaches the same end value, although it does so faster due to the higher overall rate coefficient, but a slightly larger amount of CO is formed at equilibrium (42.7% compared to 37.4%). As a result, the H_2 : CO ratio slightly changes to 0.98 at the shortest residence time, and to 0.94 at the longest. The other components remain almost constant.

Changing the CO_2 : CH_4 ratio has a large impact on the product formation, as can be seen in Figure 5(c and d). A larger fraction of CO_2 in the mixture (3:1 ratio) increases the CO fraction after a short residence time, but eventually reaches the same maximum concentration as for the 1:1 ratio, i.e. 37.1% vs. 37.4%, respectively. The H_2 concentration, on the other hand, is significantly reduced over the entire residence time by almost a third, reaching a maximum of 23.8%, compared to 39% for the 1:1 ratio. The H_2 : CO ratio therefore decreases as well, to values between 0.49 and 0.64. The higher CO_2 fraction leads to a slight increase in the O_2 concentration, which is 0.008% at the shortest residence time and 0.0114% at the longest, but is still very low compared to pure CO_2 splitting, as explained above. The concentration of the remaining components strongly decreases to values well below 1%, as can be seen in Table S 6.

Vice versa, a large fraction of CH_4 in the mixture (1:3 ratio) seems to be more beneficial overall. The CO concentrations are half the values reached for the 1:1 ratio across the entire range of residence times, but the H_2 concentration increases by a factor 1.2 to 1.5, showing a maximum of 56.1%, and thus resulting in large H_2 : CO ratios between 2.34 and 3.08, which is more optimal for the production of (oxygenated) alkanes and alkenes via the Fischer-Tropsch

process [49]. The ethane, ethene and propane production rises as well, with concentrations up to 4.02%, 0.32% and 1.43%, respectively, at 17.5 s. Higher CH_4 fractions are however more susceptible to carbon depositions, requiring periodic physical cleaning, or chemical cleaning by e.g. pure O_2 or H_2. For this reason it could be interesting to add more CO_2 in the mix, to prevent carbon deposition.

An interesting observation can be made for the CO and CO_2 concentrations. For all DRM experiments—except at a 1:3 ratio and at long residence times, when most condensable products are being made—the sum of CO_{out} and $CO_{2,out}$ after the experiment is equal to $CO_{2,in}$ before the experiment, as can be seen in Table S 6. This means that in DRM, on a global scale, all net CO_2 conversion is dominated by the transformation of CO_2 into CO, without further reaction towards hydrocarbons. It might be possible that on the molecular scale some CO reacts towards elemental C and O, or towards C1 oxygenates, and some hydrocarbons (or elemental C) partially oxidize to CO. However, on a reactor scale, CO_2, besides mainly being a source of 'non-reactive' CO, seems to act only as an oxygen source for the oxygenated hydrocarbons and water, which means that CH_4 is expected to be the actual carbon source for the production of the (oxygenated) hydrocarbons. A comparative study to partial oxidation of CH_4 ($CH_4 + O_2 \rightarrow C_xH_yO_z$) might be of interest to check the conversion efficiency (both on a rate coefficient and energy basis) towards (oxygenated) hydrocarbons.

Also, we observe that the produced fraction of CO in the empty reactor during CO_2 dissociation matches the maximum produced fractions of CO in DRM with CO_2 – CH_4 fractions of 3:1 and 1:1. As the CO_2 fraction in the mixture is reduced, the effective CO_2 conversion increases, to maintain the same overall CO_2 consumption, and thus CO production. It seems that the equilibrium concentration of CO_2 in the empty reactor, in both CO_2 dissociation and DRM, is limited to the same power-dependent maximum value of 36%, independent of the DRM ratio. Only when lowering the initial CO_2 fraction to 25%, as in the 1:3 DRM ratio, we obtain lower fractions of CO, which is logical due to the low initial concentration of CO_2. Hence, it confirms

our conclusion of no noticeable production of CO from CH_4. Also, when adding the SiO_2 packing material, we observe a higher CO production, due to the optimized kinetics, as discussed in section 3.3, although the maximum CO fraction here does not match the maximum CO fraction from SiO_2-packed CO_2 dissociation.

3.6 Further considerations

3.6.1 Strengths and limitations of this PCE study

The focus of this study is to accurately quantify the amount of (reacted) CO_2 and CH_4, as it is the input of the PCE model equation. Characterizing the other components in the reactor exhaust gas is a more difficult matter. First of all, it is impossible to know all the possible products that can be formed in the reactor beforehand, let alone quantify them all. This is because we cannot calibrate for them or collect them (in the case of solid or liquid depositions) in a reliable way; up to C7 and C4-OH were detected but only few calibrated, see table S 2 in the supplementary material.

Although we cannot determine all components, we can still correctly quantify all components for which the GC was calibrated because we measured no significant gas expansion nor contraction in the DRM and CH_4 reforming experiments; in the case of pure CO_2 dissociation we did measure gas expansion consistent with the reaction stoichiometry and this was corrected accordingly [25]. Therefore, the conversion of CH_4 and CO_2 could always be measured in a reliable way. As a result of the limited set of calibrated components, the atom balances in our experiments are not complete. Depending on the exact conditions, we missed up to 75% of a specific atom balance (most pronounced at low flow rates, SiO_2 packing, and high methane content). This is for example visible in the pure CH_4 experiments where the H_2 concentration is on average 88% of that of the converted CH_4 and thus most of the remaining CH_2 from CH_4 is missing and most likely will be deposited as liquid C_xH_y and solid C. A similar example can be seen for DRM: in section 3.5.3 we saw that, on a global reactor scale, CH_4

acted like the sole carbon source for higher hydrocarbons as equimolar amounts of CO were formed compared to the reacted CO_2. Still only a few extra (oxygenated) hydrocarbons and a minor amount of O_2 could be quantified, resulting in incomplete C, H, and O balances. Table S 9 in the supplementary material shows all atom balances for all gas mixtures and for both empty and SiO_2-packed reactors (if applicable).

Also, one can think about the validity of applying the partial chemical equilibrium (PCE) concept in these more complex chemical reactions (CH_4 reforming and DRM), in comparison to CO_2 dissociation. In the latter, CO_2 is split into CO and O_2, which are usually the only end products, unless significant O_3 or carbon deposition would be present due to some conditions. Once the CO_2 loss rate is equal to the formation rate by CO oxidation, PCE is reached and further extension of the residence time has no influence on the overall CO_2 conversion, or CO and O_2 formation. However, the chemistry in CH_4 reforming and DRM is much more complex, which means that the manifestation of the PCE might be different for each component. In sections 3.1 to 3.4, we showed that the PCE appears to be reached in CH_4 reforming and DRM, based on the CO_2 or CH_4 conversions alone. An explicit proof for the existence of a global PCE state, however, would entail running the same conversion process starting from the pure products and verifying if this results in the same final gas composition, as we did in [25]. Such an approach is precluded here by the difficulty of identifying all species in these more complex gas mixtures. As noted earlier, smaller hydrocarbons might for example still polymerize to higher hydrocarbons, while the latter can dissociate back into lower hydrocarbons, and it is not clear from our results if true equilibrium was already reached in our experiments. For this reason, the PCE analysis in this work was mostly restricted to the easy-to-characterise initial reactants. At least for these gases, time-dependent concentrations appear to be consistent with PCE behaviour, in line with our previous more rigorous investigation of the chemically more simple CO_2 dissociation process [25]. As a result, we can confidently report PCE conversions of the feed gases, but not PCE yields for all the products. Additionally, despite the

extensive nature of the (plasma) chemistry in CH_4 reforming and DRM, our results confidently prove that the overall gas conversion processes resulting from even these complex reactions can be described by our apparent first order kinetics PCE model, demonstrating opportunities towards other reaction and reactor types.

3.6.2 Interpreting the energy cost

Finally, we shortly reflect on the efficiency of the reactor configurations used in this work. For this, we invoke the concept of the energy cost (EC), i.e. the amount of energy necessary to convert one mole of reactant mixture, according to:

$$EC = \frac{SEI.V_m}{X_{Total}} \quad (11)$$

with SEI the specific energy input based on the ratio of the plasma power and $\dot{V}$ the volumetric flow rate $\left(SEI = P/\dot{V}\right)$, and V_m the molar volume (22.4 L/mol). The calculated EC for all experiments can be found in Table S 1 in the supplementary material.

The fact that the plasma conversion processes under consideration can be characterized by PCE behaviour has import consequences for their energy cost. The conversion asymptotically reaches the equilibrium conversion as an upper limit, which cannot be further improved by increasing the specific energy input (for a given set of plasma conditions). As a result, accurate determination of the location of the PCE, and the rate of evolution towards it, requires running conversion experiments at long residence time, resulting in very low energy efficiencies. However, such experiments would only have to be carried out once for a given process/reactor combination. Afterwards, the obtained information can be used to design or select an optimal process or conditions, determined by economical or practical considerations. More specifically, the rate coefficient and equilibrium conversion allow to predict the conversion as a function of residence time, which can be contrasted with energy cost at the same residence time; an optimal balance between the two can be selected, and compared with another process.

From the calculated EC data we can see that the minimum EC for almost all cases is reached at the shortest residence time (or highest flow rate), except for pure CH_4 reforming. This is due

to the fact that, generally, the conversion rises too slowly with increasing residence time, or in other words, the rate at which the flow rate decreases cannot be matched by the increase in total conversion. For CO_2 dissociation we find a minimum EC of 1.7 kWh/mol at 2.9 s, while the minimum EC of CH_4 reforming is even higher, i.e. 2.6 kWh/mol at 10 s. In both cases, adding a packing material to the reactor does not yield a lower EC. Interestingly, DRM in a 1:1 ratio shows better results, with a minimum EC of 1.16 kWh/mol at 2.9 s. Both the 3:1 and 1:3 ratios perform slightly worse, with values of 1.32 and 1.38 kWh/mmol, respectively. From these data we conclude that the most effective use of the DBD plasma reactor is at shorter residence times. This conclusion might change however if we take other aspects into account, such as separation processes and the (liquid) higher hydrocarbons. Indeed, the separation of a low converted gas mixture might suffer from high running costs, rendering less energy efficient conditions but with higher overall conversion. An optimum can probably be found here, depending on the physical process volume and process parameters. Moreover, we found in sections 3.5.2 and 3.5.3 that the longer residence times produced higher amounts of products, and also more diverse products. Depending on the desired end products, i.e. either syngas, lower hydrocarbons, or liquids, different operating conditions might be preferred. Therefore, a careful analysis of this type of experiments is very useful for the design of optimised processes for specific purposes.

4 Conclusion

In this paper we investigated the kinetics of the CO_2 dissociation and CH_4 reforming reactions and how they influence each other when both gases are combined in DRM. Fitting the time evolution of the gas composition to a new generalised first order kinetic model for the partial chemical equilibrium made it possible to determine multiple trends, elucidate macroscopic changes in the plasma chemistry, and link them to changes in the loss or formation reactions of the reagents. CO_2 dissociation exhibits a higher apparent rate coefficient (0.120 s^{-1}) than CH_4 reforming (0.041 s^{-1}), but CH_4 reforming has a higher equilibrium conversion (82%) than

CO_2 dissociation (53.6%). The lower rate coefficient of CH_4 reforming is attributed to fast dissociation and recombination reactions, rendering a slow net overall rate. Mixing both gases in a 1:1 ratio combines the best of both worlds, i.e. the higher equilibrium conversion of CH_4 reforming, yielding 75.4%, and the higher rate coefficient of CO_2 dissociation, ending up at 0.088 s^{-1}. These results point to additional interactions of the two gases, which open new pathways by the individual gas products.

Adding a spherical non-porous SiO_2 packing material to the reactor increases the electron temperature and thus further stimulates electron impact-based processes, causing gas-specific effects. In a pure CO_2 plasma, the equilibrium shifts further away to 71.1%, at the cost of slightly reducing the overall conversion rate to 0.111 s^{-1}, whereas for CH_4 reforming the equilibrium conversion stays about the same at 81% and the apparent rate coefficient increases to 0.074 s^{-1}. Mixing the gases results in an increase of both equilibrium and rate coefficient in 1:1 DRM to 84.3% and 0.130 s^{-1}, respectively.

Comparing different CO_2 : CH_4 ratios reveals the delicate balance of the combined chemistry. CO_2 drives the loss reactions in DRM, resulting in higher reaction rate coefficients when present in higher fractions; the presence of CH_4 in the mixture suppresses back reactions, resulting in higher equilibrium conversions when it is more abundant.

Finally, analysis of the effluent of all experiments revealed not only how the product composition changes and is influenced by mixing the CO_2 and CH_4, but also how it changes in time. We see trade-offs between producing larger amounts of hydrocarbons (when more CH_4 is present in the mixture), and optimal H_2 : CO syngas ratios (when more CH_4 is present).

The method for kinetic analysis used in this work is shown to be a practical way to describe the plasma-based conversion of molecules of interest in arbitrary gas mixtures with *a priori* unknown stoichiometry. In addition, we have shown how analysis of the derived kinetic parameters can elucidate key mechanistic aspects of the conversion process and help bridge

the gap with detailed kinetic models. We therefore highly advise this method for any further research in plasma (catalysis) based gas conversion.

Acknowledgements

The authors acknowledge financial support from the European Fund for Regional Development through the cross-border collaborative Interreg V program Flanders-the Netherlands (project EnOp), the Fund for Scientific Research (FWO; grant number: G.0254.14N), a TOP-BOF project and an IOF-SBO (SynCO2Chem) project from the University of Antwerp.

References

[1] H.-H. Kim, Nonthermal plasma processing for air-pollution control: A historical review, current issues, and future prospects, Plasma Process. Polym. 1 (2004) 91–110. doi:10.1002/ppap.200400028.

[2] J. Van Durme, J. Dewulf, C. Leys, H. Van Langenhove, Combining non-thermal plasma with heterogeneous catalysis in waste gas treatment: A review, Appl. Catal. B Environ. 78 (2008) 324–333. doi:10.1016/j.apcatb.2007.09.035.

[3] U. Kogelschatz, Dielectric-barrier discharges: Their history, discharge physics, and industrial applications, 23 (2003) 1–46.

[4] R. Snoeckx, A. Bogaerts, Plasma technology – a novel solution for CO_2 conversion?, Chem. Soc. Rev. 46 (2017) 5805–5863. doi:10.1039/C6CS00066E.

[5] T. Butterworth, R. Elder, R. Allen, Effects of particle size on CO_2 reduction and discharge characteristics in a packed bed plasma reactor, Chem. Eng. J. 293 (2016) 55–67. doi:10.1016/j.cej.2016.02.047.

[6] I. Michielsen, Y. Uytdenhouwen, J. Pype, B. Michielsen, J. Mertens, F. Reniers, V. Meynen, A. Bogaerts, CO_2 dissociation in a packed bed DBD reactor: First steps towards a better understanding of plasma catalysis, Chem. Eng. J. 326 (2017) 477–488. doi:10.1016/j.cej.2017.05.177.

[7] Y. Uytdenhouwen, S. Van Alphen, I. Michielsen, V. Meynen, P. Cool, A. Bogaerts, A packed-bed DBD micro plasma reactor for CO_2 dissociation: Does size matter?, Chem. Eng. J. 348 (2018) 557–568. doi:10.1016/j.cej.2018.04.210.

[8] R. Aerts, W. Somers, A. Bogaerts, Carbon Dioxide Splitting in a Dielectric Barrier Discharge Plasma: A Combined Experimental and Computational Study, ChemSusChem. 8 (2015) 702–716. doi:10.1002/cssc.201402818.

[9] X. Duan, Z. Hu, Y. Li, B. Wang, Effect of dielectric packing materials on the decomposition of carbon dioxide using DBD microplasma reactor, AIChE J. 61 (2015) 898–903. doi:10.1002/aic.

[10] D. Mei, X. Zhu, Y. He, J.D. Yan, X. Tu, Plasma-assisted conversion of CO_2 in a dielectric barrier discharge reactor: understanding the effect of packing materials, Plasma Sources Sci. Technol. 24 (2015) 15011. doi:10.1088/0963-0252/24/1/015011.

[11] X. Tu, J.C. Whitehead, Plasma-catalytic dry reforming of methane in an atmospheric dielectric barrier discharge: Understanding the synergistic effect at low temperature, Appl. Catal. B Environ. 125 (2012) 439–448. doi:10.1016/j.apcatb.2012.06.006.

[12] I. Michielsen, Y. Uytdenhouwen, A. Bogaerts, V. Meynen, Altering Conversion and Product Selectivity of Dry Reforming of Methane in a Dielectric Barrier Discharge by Changing the Dielectric Packing Material, Catalysts. 9 (2019) 51. doi:10.3390/catal9010051.

[13] R. Snoeckx, A. Rabinovich, D. Dobrynin, A. Bogaerts, A. Fridman, Plasma-based liquefaction of methane: The road from hydrogen production to direct methane liquefaction, Plasma Process. Polym. 14 (2017) e1600115. doi:10.1002/ppap.201600115.

[14] B.S. Patil, Q. Wang, V. Hessel, J. Lang, Plasma N_2-fixation: 1900–2014, Catal. Today. 256 (2015) 49–66. doi:10.1016/j.cattod.2015.05.005.

[15] M.D. Bai, X.Y. Bai, Z.T. Zhang, B. Mingdong, B. Xiyao, Z. Zhitao, Synthesis of ammonia

in a strong electric field discharge at ambient pressure, Plasma Chem. Plasma Process. 20 (2000) 511–520.

[16] A. Mizuno, Industrial applications of atmospheric non-thermal plasma in environmental remediation, Plasma Phys. Control. Fusion. 49 (2007) A1–A15. doi:10.1088/0741-3335/49/5A/S01.

[17] G.J. van Rooij, D.C.M. van den Bekerom, N. den Harder, T. Minea, G. Berden, W.A. Bongers, R. Engeln, M.F. Graswinckel, E. Zoethout, M.C.M. van de Sanden, Taming microwave plasma to beat thermodynamics in CO_2 dissociation, Faraday Discuss. 183 (2015) 233–248. doi:10.1039/c5fd00045a.

[18] A. Berthelot, A. Bogaerts, Modeling of CO_2 Splitting in a Microwave Plasma: How to Improve the Conversion and Energy Efficiency, J. Phys. Chem. C. 121 (2017) 8236–8251. doi:10.1021/acs.jpcc.6b12840.

[19] M. Ramakers, G. Trenchev, S. Heijkers, W. Wang, A. Bogaerts, Gliding Arc Plasmatron: Providing an Alternative Method for Carbon Dioxide Conversion, ChemSusChem. 10 (2017) 2642–2652. doi:10.1002/cssc.201700589.

[20] E. Cleiren, S. Heijkers, M. Ramakers, A. Bogaerts, Dry Reforming of Methane in a Gliding Arc Plasmatron: Towards a Better Understanding of the Plasma Chemistry, ChemSusChem. (2017). doi:10.1002/cssc.201701274.

[21] T. Mizushima, K. Matsumoto, J.I. Sugoh, H. Ohkita, N. Kakuta, Tubular membrane-like catalyst for reactor with dielectric-barrier- discharge plasma and its performance in ammonia synthesis, Appl. Catal. A Gen. 265 (2004) 53–59. doi:10.1016/j.apcata.2004.01.002.

[22] M. Bai, Z. Zhang, X. Bai, M. Bai, W. Ning, Plasma Synthesis of Ammonia With a Microgap Dielectric Barrier Discharge at Ambient Pressure, IEEE Trans. Plasma Sci. 31 (2003) 1285–1291. doi:10.1109/TPS.2003.818761.

[23] Q. Wang, Y. Cheng, Y. Jin, Dry reforming of methane in an atmospheric pressure

plasma fluidized bed with Ni/γ-Al_2O_3 catalyst, Catal. Today. 148 (2009) 275–282. doi:10.1016/j.cattod.2009.08.008.

[24] A. Huang, G. Xia, J. Wang, S.L. Suib, Y. Hayashi, H. Matsumoto, CO_2 reforming of CH_4 by atmospheric pressure AC discharge plasmas, J. Catal. 189 (2000) 349–359. doi:10.1006/jcat.1999.2684.

[25] Y. Uytdenhouwen, K.M. Bal, I. Michielsen, E.C. Neyts, V. Meynen, P. Cool, A. Bogaerts, How process parameters and packing materials tune chemical equilibrium and kinetics in plasma-based CO_2 conversion, Chem. Eng. J. 372 (2019) 1253–1264. doi:10.1016/j.cej.2019.05.008.

[26] J.C. Whitehead, Plasma – catalysis : the known knowns , the known unknowns and the unknown unknowns, J. Phys. D. Appl. Phys. 49 (2016) 243001. doi:10.1088/0022-3727/49/24/243001.

[27] X. Tu, H.J. Gallon, M. V Twigg, P. a Gorry, J.C. Whitehead, Catalyst in a Coaxial Dielectric Barrier Discharge Reactor, J. Phys. D. Appl. Phys. 44 (2011) 274007. doi:10.1088/0022-3727/44/27/274007.

[28] T. Nozaki, K. Okazaki, Non-thermal plasma catalysis of methane: Principles, energy efficiency, and applications, Catal. Today. 211 (2013) 29–38. doi:10.1016/j.cattod.2013.04.002.

[29] S. Vepřek, Statistical model of chemical reactions in nonisothermal low pressure plasma, J. Chem. Phys. 57 (1972) 952–959. doi:10.1063/1.1678345.

[30] S. Vepřek, W. Peier, Chemical equilibrium in nonisothermal low pressure plasma, Chem. Phys. 2 (1973) 478–484. doi:10.1016/0301-0104(73)80024-2.

[31] J.J. Wagner, S. Vepřek, Kinetic study of the heterogeneous Si/H system under low-pressure plasma conditions by means of mass spectrometry, Plasma Chem. Plasma Process. 2 (1982) 95–107. doi:10.1007/BF00566860.

[32] C. De Bie, B. Verheyde, T. Martens, J. Van Dijk, S. Paulussen, A. Bogaerts, Fluid

modeling of the conversion of methane into higher hydrocarbons in an atmospheric pressure dielectric barrier discharge, Plasma Process. Polym. 8 (2011) 1033–1058. doi:10.1002/ppap.201100027.

[33] C. Xu, X. Tu, Plasma-assisted methane conversion in an atmospheric pressure dielectric barrier discharge reactor, J. Energy Chem. 22 (2013) 420–425. doi:10.1016/S2095-4956(13)60055-8.

[34] Y. Gao, S. Zhang, H. Sun, R. Wang, X. Tu, T. Shao, Highly efficient conversion of methane using microsecond and nanosecond pulsed spark discharges, Appl. Energy. 226 (2018) 534–545. doi:10.1016/j.apenergy.2018.06.006.

[35] Y. Yang, Direct Non-oxidative Methane Conversion by Non-Thermal Plasma: Experimental Study, Plasma Chem. Plasma Process. 23 (2003) 283–296. doi:10.1023/A:1022968002315.

[36] A. Indarto, Hydrogen production from methane in a dielectric barrier discharge using oxide zinc and chromium as catalyst, J. Chinese Inst. Chem. Eng. 39 (2008) 23–28. doi:10.1016/j.jcice.2007.10.001.

[37] Z.A. Allah, J.C. Whitehead, Plasma-catalytic dry reforming of methane in an atmospheric pressure AC gliding arc discharge, Catal. Today. 256 (2015) 76–79. doi:10.1016/j.cattod.2015.03.040.

[38] X. Tu, J.C. Whitehead, Plasma-catalytic dry reforming of methane in an atmospheric dielectric barrier discharge: Understanding the synergistic effect at low temperature, Appl. Catal. B Environ. 125 (2012) 439–448. doi:10.1016/j.apcatb.2012.06.006.

[39] W.C. Chung, M.B. Chang, Review of catalysis and plasma performance on dry reforming of CH_4 and possible synergistic effects, Renew. Sustain. Energy Rev. 62 (2016) 13–31. doi:10.1016/j.rser.2016.04.007.

[40] R. Snoeckx, Y.X. Zeng, X. Tu, A. Bogaerts, Plasma-based dry reforming: improving the conversion and energy efficiency in a dielectric barrier discharge, RSC Adv. 5 (2015)

29799–29808. doi:10.1039/C5RA01100K.

[41] A. Bogaerts, C. De Bie, R. Snoeckx, T. Kozák, Plasma based CO_2 and CH_4 conversion: A modeling perspective, Plasma Process. Polym. 14 (2017). doi:10.1002/ppap.201600070.

[42] R. Snoeckx, R. Aerts, X. Tu, A. Bogaerts, Plasma-Based Dry Reforming: A Computational Study Ranging from the Nanoseconds to Seconds Time Scale, J. Phys. Chem. C. 117 (2013) 4957–4970. doi:10.1021/jp311912b.

[43] C. De Bie, J. Van Dijk, A. Bogaerts, The Dominant Pathways for the Conversion of Methane into Oxygenates and Syngas in an Atmospheric Pressure Dielectric Barrier Discharge, J. Phys. Chem. C. 119 (2015) 22331–22350. doi:10.1021/acs.jpcc.5b06515.

[44] L. Wang, Y. Yi, C. Wu, H. Guo, X. Tu, One-step reforming of CO_2 and CH_4 into high-value liquid chemicals and fuels at room temperature by plasma-driven catalysis, Angew. Chemie - Int. Ed. 56 (2017) 13679–13683. doi:10.1002/anie.201707131.

[45] N. Pinhão, A. Moura, J.B. Branco, J. Neves, Influence of gas expansion on process parameters in non-thermal plasma plug-flow reactors: A study applied to dry reforming of methane, Int. J. Hydrogen Energy. 41 (2016) 9245–9255. doi:10.1016/j.ijhydene.2016.04.148.

[46] E.C. Neyts, A. Bogaerts, Understanding plasma catalysis through modelling and simulation—a review, J. Phys. D. Appl. Phys. 47 (2014) 224010. doi:10.1088/0022-3727/47/22/224010.

[47] K. Van Laer, A. Bogaerts, Influence of gap size and dielectric constant of the packing material on the plasma behaviour in a packed bed DBD reactor: A fluid modelling study, Plasma Process. Polym. 14 (2017) 1600129. doi:10.1002/ppap.201600129.

[48] A.S. Morillo-Candas, C. Drag, J. Booth, T.C. Dias, V. Guerra, O. Guaitella, Oxygen atom kinetics in CO_2 plasmas ignited in a DC glow discharge, Plasma Sources Sci. Technol. 28 (2019) 075010. doi:10.1088/1361-6595/ab2b84.

[49] T. Kaneko, F. Derbyshire, E. Makino, D. Gray, M. Tamura, K. Li, Coal Liquefaction, in: Ullmann's Encycl. Ind. Chem., Wiley-VCH Verlag GmbH & Co. KGaA, Weinheim, Germany, 2012: p. 96. doi:10.1002/14356007.a07_197.pub2.